High-Frequency, Long-Range Coupling Between Prefrontal and Visual Cortex During Attention

Georgia G. Gregoriou,[1]* Stephen J. Gotts,[2]* Huihui Zhou,[1] Robert Desimone[1]†

Electrical recordings in humans and monkeys show attentional enhancement of evoked responses and gamma synchrony in ventral stream cortical areas. Does this synchrony result from intrinsic activity in visual cortex or from inputs from other structures? Using paired recordings in the frontal eye field (FEF) and area V4, we found that attention to a stimulus in their joint receptive field leads to enhanced oscillatory coupling between the two areas, particularly at gamma frequencies. This coupling appeared to be initiated by FEF and was time-shifted by about 8 to 13 milliseconds across a range of frequencies. Considering the expected conduction and synaptic delays between the areas, this time-shifted coupling at gamma frequencies may optimize the postsynaptic impact of spikes from one area upon the other, improving cross-area communication with attention.

A typical crowded scene contains many objects that cannot be processed simultaneously, thus requiring attentional mechanisms to select the ones most relevant to behavior. Electrophysiological studies in monkeys have shown that attention leads to enhanced responses of neurons in ventral stream areas that are important for object recognition, at the expense of responses to distracting stimuli (*1*). Moreover, attention increases neural synchrony, often in the gamma frequency range (*2*–*5*). Given that cells have limited integration times, increases in synchrony and firing rates may together have a larger impact on downstream neurons and thus increase the effectiveness of behaviorally relevant stimuli (*6*, *7*). Areas in the prefrontal cortex (PFC) and parietal cortex may be sources of the top-down attentional feedback to ventral stream areas, which could enhance firing rates with attention (*1*, *4*, *8*). However, the mechanisms that cause increases in neural synchrony with attention in visual cortex are unknown.

We investigated whether the frontal eye field (FEF), an area within the PFC, is a source of enhanced neural synchrony effects in area V4 during attention. The FEF has reciprocal connections with V4 (*9*–*11*), and electrical stimulation of FEF enhances V4 neuronal responses to a stimulus in the receptive field (RF) (*12*, *13*). We recorded spikes (multi-unit) and local field potentials (LFPs) simultaneously from FEF and V4 in two monkeys trained in a covert attention task (Fig. 1A) (*14*). One grating stimulus appeared inside the shared RF, and two others appeared outside. After a variable delay, the spot at fixation changed color (which was the cue) so as to match the color of one of the three gratings, indicating the target stimulus to be attended. The monkey was rewarded for releasing a bar when the target stimulus changed color.

We first verified that attention caused enhanced firing rates in FEF and V4. We recorded from 292 sites with visual responses in FEF and 262 sites in V4. The results were qualitatively similar (and statistically significant) in both monkeys and were therefore combined. Figure 1, B and C, shows the average normalized response of the population of FEF and V4 neurons, respectively, for conditions with overlapping RFs. Neuronal responses were significantly increased by attention to the joint RF in both areas (average response in a window 100 to 800 ms after cue onset; Wilcoxon sign-rank test, $P < 0.001$) and remained significantly enhanced until the end of the trial (average response in a window 500 ms before the target's color change; Wilcoxon sign-rank test, $P < 0.001$) [for the distribution of attentional effects on firing rate, see the supporting online material (SOM) text].

Attentional effects on firing rates occurred significantly earlier in FEF than in V4 (at 80 ms after the cue in FEF, and 130 ms after the cue in V4) [Fig. 1, B and C dashed lines; $P = 0.017$ two-sided permutation test (SOM text)]. The distribution of attentional latencies is shown separately for FEF and V4 in Fig. 1, D and E, and was similarly shifted earlier for FEF (Wilcoxon rank-sum test, $P < 0.001$) (for a table of latency measurements, see table S1).

We next used multi-taper spectral methods to calculate the coherence between spikes and LFPs (*14*). Spike-field coherence in the gamma band significantly increased with attention within each area (coherence averaged between 40 and 60 Hz; paired t test, $P < 0.001$ in both areas), whereas low frequencies were desynchronized (average coherence between 5 and 20 Hz; paired t test, $P < 0.001$ in both areas) (Fig. 2, A and B). At the population level, gamma band coherence increased by 14% in V4 (*2*, *3*, *15*) and by 22% in the FEF (for distributions of effects, see SOM text).

If FEF is the source of enhanced synchrony in V4, the critical question is whether attention

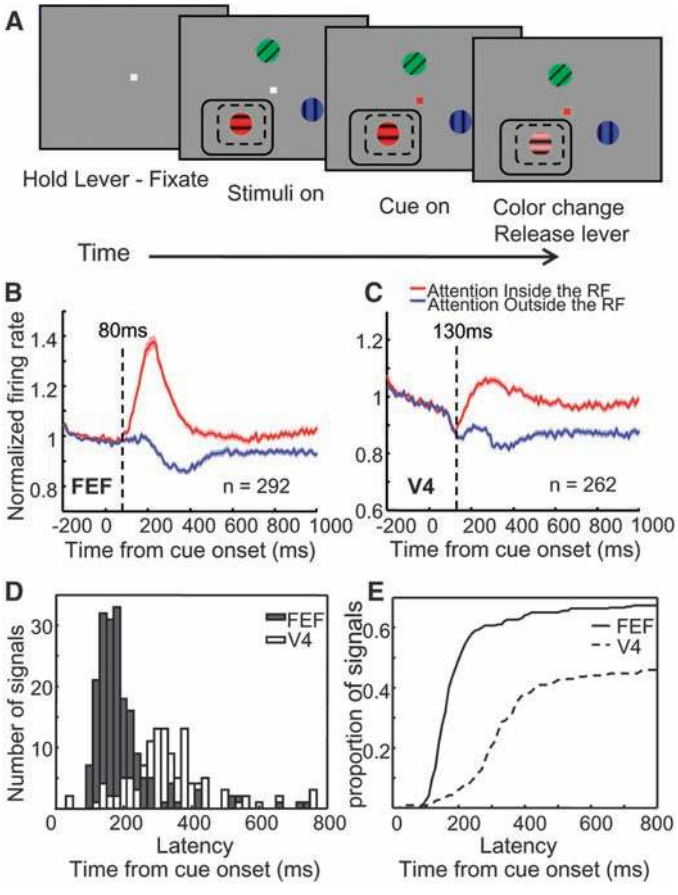

Fig. 1. (**A**) Illustration of behavioral task. Dashed- and solid-line rectangles indicate hypothetical overlapping RFs for V4 and FEF sites, respectively. (**B** and **C**) Normalized firing rates averaged across the population of cells in FEF and V4, respectively. SEM (±) at each time point is indicated by shading over the lines. Vertical dashed lines indicate latency of attentional effects at the population level. (**D**) Distribution of attentional latencies in the firing rates of FEF and V4 neurons. (**E**) Cumulative distribution of FEF and V4 latencies, represented as a proportion of recordings in which latencies could be reliably estimated.

[1]McGovern Institute for Brain Research, Massachusetts Institute of Technology, Cambridge, MA 02139, USA. [2]Laboratory of Brain and Cognition, National Institute of Mental Health, National Institutes of Health, Bethesda, MD 20892, USA.

*These authors contributed equally to this work.
†To whom correspondence should be addressed. E-mail: desimone@mit.edu

increases coupled oscillations between the two areas. We found that the attentional effect on gamma frequency spike-field coherence between areas was even larger than the effects within areas (Fig. 2, C and D). With attention, gamma coherence between V4 spikes and FEF LFPs increased by 26% at the population level (paired t test, $P < 0.001$), between FEF spikes and V4 LFPs increased by 37% (paired t test, $P < 0.001$), and remained enhanced through the end of the trial (paired t test, $P < 0.001$ for all pair types). All of these effects were highly dependent on RF overlap at the locus of attention. For pairs of recordings with nonoverlapping RFs, coherence in the two attention conditions did not differ from that in the pre-stimulus period (one-way analysis of variance, $P = 0.86$) (Fig. 2F and SOM text).

Gamma frequency coherence between LFPs recorded across the two areas was enhanced 63% by attention (Fig. 2E) (paired t test, $P < 0.001$), and gamma coherence between spike trains across areas was enhanced by 13% (paired t test, $P < 0.001$). In general, spike-spike coherence across electrodes is smaller than spike-field and field-field coherence for statistical reasons (*16*). Another probable factor is that connections between FEF and V4 are patchy (*9*, *10*), and LFPs sum signals over a wider area.

We considered whether the synchronous oscillations between V4 and FEF might have resulted from a common oscillatory input, which would be expected to result in zero phase-lag synchrony between the areas. To test for this, we computed the distribution of the coherence phase shifts within and across areas. Within areas, the distribution of the average (between 40 and 60 Hz) relative phase between the two recorded signals (Fig. 3) had a median close to zero (attend-in condition; Rayleigh test, FEF, $P < 0.001$, median = 7°, and V4, $P < 0.001$, median = –26°), corresponding to a time delay of 0.5 to 1.5 ms between spikes and the phase of maximum depolarization in the LFP at 50 Hz (Fig. 3A). By contrast, the phase of spike-field coherence across areas was shifted approximately half a gamma cycle [attend-in condition; Rayleigh test, FEF spikes–V4 LFPs, $P < 0.001$, median phase = –142° (or 218°), and V4 spikes–FEF LFPs, $P < 0.001$, median phase = 144° (or –216°)], corresponding to a time shift of ~8 (or 12) ms (Fig. 3A). Likewise, the median phase of spike-spike coherence pairs having a maximum gamma coherence peak of at least 0.1 was about 120°, which corresponds to a time shift of 7 ms. Similar results were found by com-

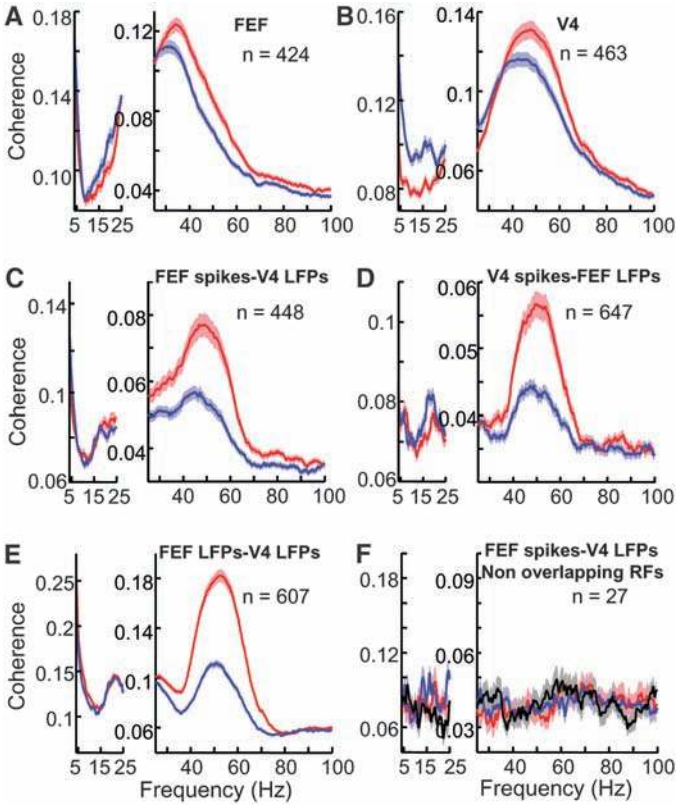

Fig. 2. Attentional enhancement of synchronization. (**A** to **D**) Spike-field coherence (A) within FEF, (B) within V4, (C) between spikes in FEF and LFPs in V4, and (D) between spikes in V4 and LFPs in FEF. (**E**) LFP-LFP coherence between FEF and V4 sites. Conventions are the same as in Fig. 1. (**F**) Spike-LFP coherence between FEF spikes and V4 LFPs from recording sites with nonoverlapping RFs (i) with attention inside the V4 RF during the post-stimulus period (red line), (ii) with attention in right hemifield, outside both V4 and FEF RFs during the post-stimulus period (blue line), and (iii) during the pre-stimulus period with no stimuli except for the fixation spot (black line). Tapers providing an effective smoothing of ±10 Hz were used for spectral estimation of higher frequencies [25 to 100 Hz, right part of (A) to (F)] and tapers providing smoothing of ±3 Hz were used for lower frequencies [<25 Hz, left part of (A) to (F)].

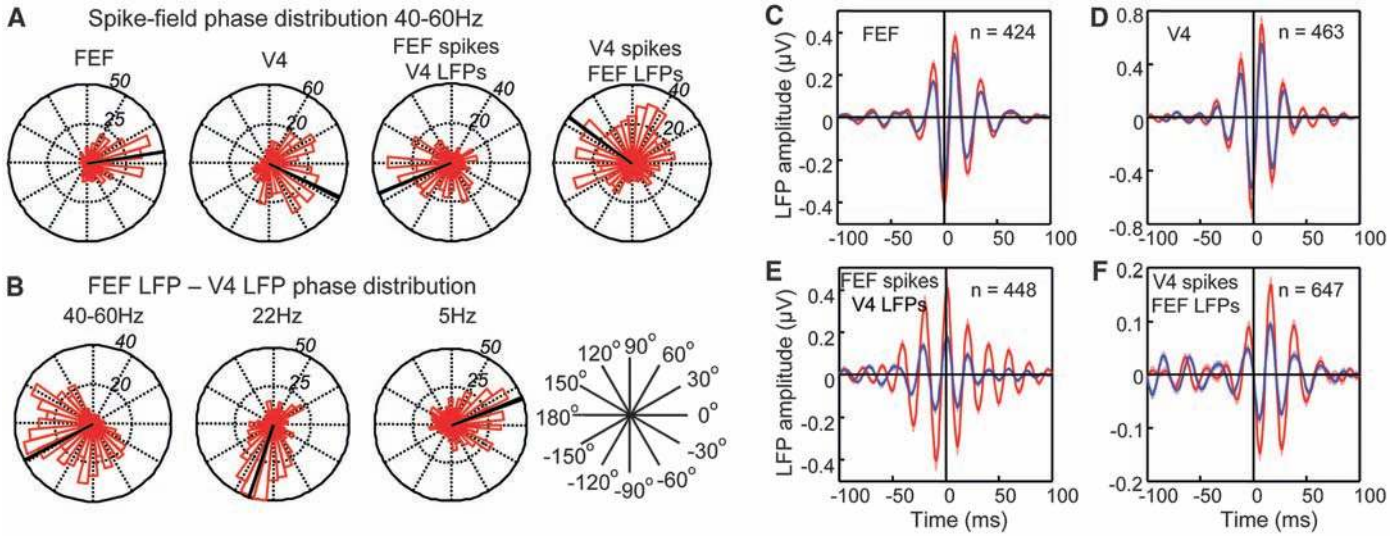

Fig. 3. Relative phase. (**A**) Distribution of average relative phase (40 to 60 Hz) between spikes and LFPs within and across areas. (**B**) Distribution of relative phases between FEF and V4 LFPs at different frequencies (40 to 60 Hz, 22 Hz, and 5 Hz). Shown are all phases from condition with attention inside the RF. (**C** to **F**) Spike-triggered averages of LFPs filtered between 35 and 80 Hz with (C) spikes and LFPs from FEF, (D) spikes and LFPs from V4, (E) spikes from FEF and LFPs from V4, and (F) spikes from V4 and LFPs from FEF. Conventions are the same as in Fig. 1.

paring spike-triggered averages of the LFP within and across areas (Fig. 3, C to F).

Although the peak coherence and largest attentional effects were in the gamma range, there was also coherence between FEF and V4 at other frequencies. We therefore tested whether the phase relationship at these other frequencies followed a fixed time shift of ~8 to 12 ms or a fixed phase shift of half a cycle. The medians of the distributions for the gamma, beta, and theta frequencies (40- to 60-Hz median = –152°, 22-Hz median = –105°, and 5-Hz median = 20°) correspond to time delays of –8, –13, and 11 ms, or a relatively fixed time shift of 8 to 13 ms in either direction rather than a fixed phase shift (Fig. 3B). A comparable (~10 ms) delay has been found between visual response latencies in anatomically connected areas along the ventral stream (*17*), suggesting that conduction times and synaptic delays account for the 8 to 13 ms shift in coupling.

The earlier latency of attentional effects on firing rates in FEF as compared with those in V4 suggests that FEF may initiate the coupled oscillations between the two areas. To further test this idea, we used Granger causality analysis to test the relative strength of influence of V4 on FEF LFPs and vice versa (*14*). Granger causality values for gamma increased with attention for both directions (paired t test, $P < 0.001$ for both directions) and were significantly above chance (FEF → V4 peak = 0.010 at 46 Hz and V4 → FEF peak = 0.025 at 55 Hz; permutation test, $P < 0.001$) (*14*), indicating that gamma activity in each area has a significant causal influence on the other area. However, the attentional effects on the Granger causality values appeared significantly earlier in the FEF-to-V4 direction than in the reverse direction (FEF to V4, 110 ms, and V4 to FEF, 160 ms; two-sided permutation test, $P < 0.05$) (Fig. 4, A and B), which is consistent with the idea that FEF initiates the gamma frequency oscillations in V4. The causality relationship reversed a short time later, with the Granger values becoming significantly larger in the V4-to-FEF direction around 300 ms after the cue onset (average 400 to 1000 ms after cue onset; paired t test, $P < 0.001$). In fact, the Granger values in the FEF-to-V4 direction greatly diminished across the trial.

We considered whether firing-rate changes with attention in FEF preceded the attentional effects on synchrony or vice versa. We used the Hilbert-Huang transform method (*18*) to calculate instantaneous LFP power over time in FEF and V4 (Fig. 4C). At the population level, significant attentional enhancement of gamma power in the LFP in FEF and V4 occurred at 120 ms and 100 ms, respectively (Fig. 4D), which was not a significant difference (two-sided permutation test, $P = 0.84$). To compare the relative latencies of attention effects on firing rate and LFP gamma power, we calculated the distribution of latencies for attentional effects across all individual sites in the first 300 ms after the cue onset. The distributions of attentional latencies in LFP gamma power in both FEF and V4 were significantly later than the distribution of latencies for attentional effects on firing rates in FEF (Wilcoxon rank-sum test, $P < 0.01$ for both comparisons) and significantly earlier than the distribution of latencies for attentional effects on V4 firing rates (Wilcoxon rank-sum test; V4 LFP gamma power, $P < 0.05$, and FEF LFP gamma power, $P < 0.001$) (table S2). Together, these results indicate that significant attentional effects on LFP gamma power in either area occur later than the earliest attentional effects on firing rates in the FEF. Rather than being caused by enhanced gamma oscillations, increases in firing rates in FEF with attention may initiate the coupled oscillations within and across areas. In contrast, firing-rate changes in area V4 occur later and might result at least in part from enhanced gamma oscillations.

In summary, the results suggest that FEF is a major source of the attentional effects on gamma frequency synchrony in V4 and probably other ventral stream areas. The Granger causality analyses suggest that top-down inputs from FEF to V4 predominate at the onset of spatially directed attention, but the bottom-up inputs from V4 to FEF come to predominate over the course of sustained attention. The coupled oscillations across areas are shifted in time by about 8 to 13 ms, which may be the optimal time shift to allow for spikes initiated in one area to affect cells at a peak depolarization phase in the coupled area (*17*). Tight coupling between the inputs and outputs of cells in V4 and FEF may also allow for enhanced spike timing–dependent plasticity of the connections between the two areas (*19*), which might mediate learning effects with attention. For distracting stimuli, or for sites with nonoverlapping RFs, these coupled oscillations are much smaller, which will reduce the impact of spikes in one area upon the other. We do not suggest that the attentional effects on gamma synchrony and firing rates in V4 are caused solely by inputs from FEF, because V4 receives inputs from several other structures that have been implicated in attention (*1*). However, these other inputs may also need to be synchronized at compatible frequencies and with the appropriate time shifts in order to support effective communication.

It has been suggested that low-frequency synchronization (for example, beta) is more suitable for long-range or polysynaptic communication across distant brain areas, with gamma rhythms being used for local computations (*20*). Although there is evidence for such low-frequency long-range synchronization (*21*–*25*), here we show that two distant but monosynaptically connected areas can be synchronized at gamma frequencies, which is probably not caused simply by common input (*21*). Enhanced oscillatory coupling has now been reported across several brain structures in monkeys (*4*, *23*, *26*) and other species (*21*, *24*, *27*) in association with attention and other behaviors, at a variety of frequencies, and may therefore be a general mechanism for regulating communication across brain structures (*6*, *28*).

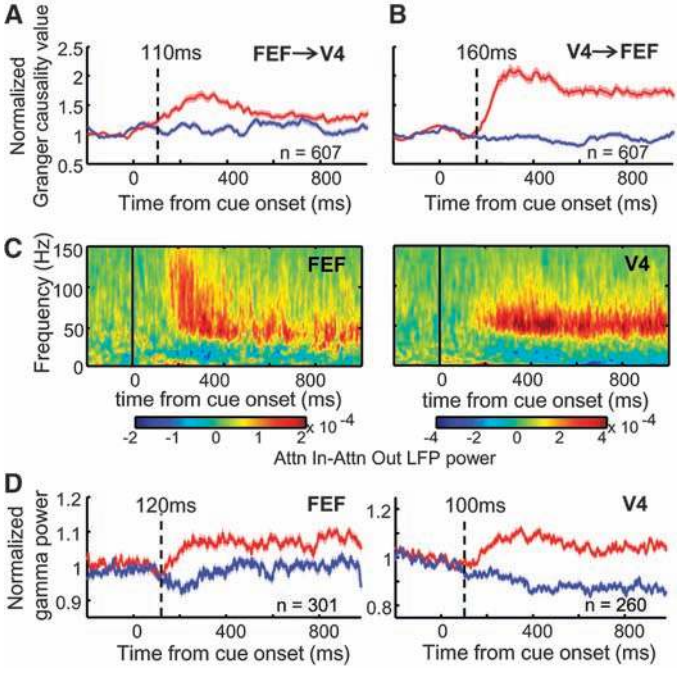

Fig. 4. Time-frequency synchrony measures and directional influences. (**A** and **B**) Population average of normalized Granger causality values averaged between 40 and 60 Hz across all pair-wise combinations of LFPs recorded in FEF and V4. Direction of influence is indicated by the arrows. (**C**) Population averages of attentional effects (attention inside RF–attention outside RF) on FEF and V4 power. (**D**) Normalized LFP gamma power in FEF and V4. Conventions are the same as in Fig. 1.

References and Notes

1. R. Desimone, J. Duncan, *Annu. Rev. Neurosci.* **18**, 193 (1995).
2. P. Fries, J. H. Reynolds, A. E. Rorie, R. Desimone, *Science* **291**, 1560 (2001).
3. N. P. Bichot, A. F. Rossi, R. Desimone, *Science* **308**, 529 (2005).
4. Y. B. Saalmann, I. N. Pigarev, T. R. Vidyasagar, *Science* **316**, 1612 (2007).
5. P. Lakatos, G. Karmos, A. D. Mehta, I. Ulbert, C. E. Schroeder, *Science* **320**, 110 (2008).
6. C. Borgers, S. Epstein, N. J. Kopell, *Proc. Natl. Acad. Sci. U.S.A.* **105**, 18023 (2008).
7. P. Tiesinga, J. M. Fellous, T. J. Sejnowski, *Nat. Rev. Neurosci.* **9**, 97 (2008).
8. E. K. Miller, J. D. Cohen, *Annu. Rev. Neurosci.* **24**, 167 (2001).
9. G. B. Stanton, C. J. Bruce, M. E. Goldberg, *J. Comp. Neurol.* **353**, 291 (1995).
10. J. D. Schall, A. Morel, D. J. King, J. Bullier, *J. Neurosci.* **15**, 4464 (1995).
11. L. G. Ungerleider, T. W. Galkin, R. Desimone, R. Gattass, *Cereb. Cortex* **18**, 477 (2008).

12. T. Moore, K. M. Armstrong, *Nature* **421**, 370 (2003).
13. L. B. Ekstrom, P. R. Roelfsema, J. T. Arsenault, G. Bonmassar, W. Vanduffel, *Science* **321**, 414 (2008).
14. Materials and methods are available as supporting material on *Science* Online.
15. P. Fries, T. Womelsdorf, R. Oostenveld, R. Desimone, *J. Neurosci.* **28**, 4823 (2008).
16. M. Zeitler, P. Fries, S. Gielen, *Neural Comput.* **18**, 2256 (2006).
17. L. G. Nowak, J. Bullier, in *Cerebral Cortex*, K. S. Rockland, J. H. Kaas, A. Peters, Eds. (Plenum, New York, 1997), vol. 12, pp. 205–241.
18. N. E. Huang *et al.*, *Proc. R. Soc. London Ser. A* **454**, 903 (1998).
19. Y. Dan, M. M. Poo, *Neuron* **44**, 23 (2004).
20. N. Kopell, G. B. Ermentrout, M. A. Whittington, R. D. Traub, *Proc. Natl. Acad. Sci. U.S.A.* **97**, 1867 (2000).
21. A. von Stein, C. Chiang, P. Konig, *Proc. Natl. Acad. Sci. U.S.A.* **97**, 14748 (2000).
22. A. Brovelli *et al.*, *Proc. Natl. Acad. Sci. U.S.A.* **101**, 9849 (2004).
23. B. Pesaran, M. J. Nelson, R. A. Andersen, *Nature* **453**, 406 (2008).
24. P. R. Roelfsema, A. K. Engel, P. Konig, W. Singer, *Nature* **385**, 157 (1997).
25. A. Sirota *et al.*, *Neuron* **60**, 683 (2008).
26. T. J. Buschman, E. K. Miller, *Science* **315**, 1860 (2007).
27. A. G. Siapas, E. V. Lubenov, M. A. Wilson, *Neuron* **46**, 141 (2005).
28. T. Womelsdorf, P. Fries, *Curr. Opin. Neurobiol.* **17**, 154 (2007).
29. We thank G. Pielli, D. Stock, and C. Alfes for help with the animal training and Z.-X. Liu for help with the Granger causality analysis. We also thank N. Bichot, R. Landman, G. Mulliken, and A. Mitz for helpful discussions. Supported by grants EY017292 and EY017921 to R.D. S.J.G. was supported in part by grant MH64445 from NIH (USA).

Supporting Online Material

www.sciencemag.org/cgi/content/full/324/5931/1207/DC1
Materials and Methods
SOM Text
Figs. S1 to S5
Table S1
References

26 January 2009; accepted 8 April 2009
10.1126/science.1171402

Genome-Wide Identification of Human RNA Editing Sites by Parallel DNA Capturing and Sequencing

Jin Billy Li,[1]* Erez Y. Levanon,[1]* Jung-Ki Yoon,[1]† John Aach,[1] Bin Xie,[2] Emily LeProust,[3] Kun Zhang,[1]‡ Yuan Gao,[2,4] George M. Church[1]§

Adenosine-to-inosine (A-to-I) RNA editing leads to transcriptome diversity and is important for normal brain function. To date, only a handful of functional sites have been identified in mammals. We developed an unbiased assay to screen more than 36,000 computationally predicted nonrepetitive A-to-I sites using massively parallel target capture and DNA sequencing. A comprehensive set of several hundred human RNA editing sites was detected by comparing genomic DNA with RNAs from seven tissues of a single individual. Specificity of our profiling was supported by observations of enrichment with known features of targets of adenosine deaminases acting on RNA (ADAR) and validation by means of capillary sequencing. This efficient approach greatly expands the repertoire of RNA editing targets and can be applied to studies involving RNA editing–related human diseases.

Adenosine-to-inosine (A-to-I) RNA editing converts a genomically encoded adenosine (A) into inosine (I), which in turn is read as guanosine (G), and increases transcriptomic diversity (*1*, *2*). It is critical for normal brain function (*3*–*7*) and is linked to various disorders (*8*). To date, a total of 13 edited genes have been identified within nonrepetitive regions of the human genome (table S1). The limiting factor in the identification of RNA editing targets has been the number of locations that could be profiled by the sequencing of DNA and RNA samples. Even with recent developments in massively parallel DNA sequencing technologies (*9*), it still remains expensive to sequence whole genomes and transcriptomes, both of which are required to identify RNA editing targets. Here, we report an efficient and unbiased genome-wide approach to identify RNA editing sites that uses tailored target capture followed by massively parallel DNA sequencing.

We first compiled a set of 59,437 genomic locations enriched with RNA editing sites, excluding repetitive regions such as *Alu* (fig. S1) (*10*). To reduce biases in detection, the key criteria for previous predictions of editing targets—conservation, coding potential, and RNA secondary structure (*11*–*15*)—were not taken into account. Over 90% of the previously identified editing targets are present in this data set (table S1). We designed padlock probes (*16*) for 36,208 sites that best satisfied our criteria for probe design (table S2) (*10*). Sites near splicing junctions required two different probes [targeting genomic DNA (gDNA) and cDNA], giving rise to a total of 41,046 probes designed for 36,208 sites (table S2).

To identify RNA editing sites, we used gDNA and cDNA from seven different tissues (cerebellum, frontal lobe, corpus callosum, diencephalon, small intestine, kidney, and adrenal), all derived from a single individual so as to rule out polymorphisms among populations. The pool of probes was hybridized to gDNA and cDNA in separate reactions (Fig. 1A and fig. S2). We sequenced the amplicons and identified sites where an A allele was observed in gDNA, whereas at least a fraction of G reads were present in the cDNA samples. A majority of sites were covered with multiple reads (Fig. 1B). Two independent

Table 1. Statistics of sequencing of samples used in this study.

Sample	Total reads	Mappable reads	Sites with ≥1 read	Fraction of sites with ≥1 read	RNA editing candidates*
gDNA (combined)	12,604,941	12,150,194	33,886	93.6%	N/A
Replicate 1	5,145,193	5,042,006	32,491	89.7%	N/A
Replicate 2	7,459,748	7,108,188	32,942	91.0%	N/A
cDNA					
Cerebellum	5,538,459	5,382,743	26,220	72.4%	126
Frontal lobe (combined)	14,065,388	13,360,868	28,382	78.4%	268
Replicate 1	6,950,660	6,563,630	26,617	73.5%	238
Replicate 2	7,114,728	6,797,238	26,628	73.5%	230
Corpus callosum	5,096,832	4,963,983	25,447	70.3%	180
Diencephalon	5,420,151	5,291,184	25,187	69.6%	172
Small intestine	6,516,258	6,172,901	26,845	74.1%	181
Kidney	6,354,025	5,984,709	26,299	72.6%	177
Adrenal	2,251,755	2,188,637	23,589	65.1%	121

*A site with evidence for RNA editing is required to have an editing level of ≥5% and a log-likelihood (LL) score of ≥2 (*10*).

[1]Department of Genetics, Harvard Medical School, 77 Avenue Louis Pasteur, Boston, MA 02115, USA. [2]Center for the Study of Biological Complexity, Virginia Commonwealth University, 1000 West Cary Street, Richmond, VA 23284, USA. [3]Genomics Solution Unit, Agilent Technologies, 5301 Stevens Creek Boulevard, Santa Clara, CA 95051, USA. [4]Department of Computer Science, Virginia Commonwealth University, 401 West Main Street, Richmond, VA 23284, USA.

*These authors contributed equally to this work.
†Present address: College of Medicine, Seoul National University, Seoul 110-799, Korea.
‡Present address: Department of Bioengineering, University of California, San Diego, CA 92093, USA.
§To whom correspondence should be addressed. E-mail: http://arep.med.harvard.edu/gmc/email.html

www.sciencemag.org/cgi/content/full/324/5931/1207/DC1

Supporting Online Material for

High-Frequency, Long-Range Coupling Between Prefrontal and Visual Cortex During Attention

Georgia G. Gregoriou, Stephen J. Gotts, Huihui Zhou, Robert Desimone*

*To whom correspondence should be addressed. E-mail: desimone@mit.edu

Published 29 May 2009, *Science* **324**, 1207 (2009)
DOI: 10.1126/science.1171402

This PDF file includes:

SUPPORTING ONLINE MATERIAL

Materials and methods

Two male rhesus monkeys (*Macaca mulatta*) weighing 8-10 kg were anesthetized and were implanted under aseptic conditions with a post to fix the head and two recording chambers, one over the frontal eye field (FEF) and one over area V4. Localization of the areas was based on MRI scans obtained before surgery. All procedures and animal care were in accordance with the NIH guidelines.

Behavioral Task

The monkeys were sitting in front of a computer monitor (resolution 800x600 pixels and refresh rate 100Hz) at a distance of 57cm. Presentation of stimuli and behavioral parameters were controlled by the CORTEX software package (www.cortex.salk.edu). Eye position was monitored by an infrared based eye-tracking system at 60 Hz (ISCAN)

Monkeys had to hold a bar to initiate the trial. A fixation spot ($0.4x0.4^o$) appeared at the center of the screen, and the monkeys had to keep their gaze within a 3x3 deg window centered on the fixation spot and maintain fixation for 1500 ms, or the trial was aborted. Following successful fixation, three isoluminant, sinusoidal, drifting gratings (2^o diameter, drifting rate 1cycle/s), one red, one blue and one green, appeared on the screen. The stimuli were presented at the same distance from the center of the screen (at approximately 5^o, range 4-8^o) and they were distributed radially around the fixation point at 120^o intervals. After a variable period of time (0-1000 ms), the fixation spot was replaced by a small square cue that matched the color of one of the gratings and indicated the color of the stimulus to be attended. The monkeys shifted their attention to the target stimulus and monitored the target for a color change while maintaining fixation of the cue. By examining neural responses after the cue onset, we could measure "pure" attentional effects on responses, without interference from the strong transient visual responses to the onset of the gratings. The color change could occur as early as 250 ms and as late as 3000 ms after cue onset. When the target changed color, the animals were rewarded with a drop of juice for releasing the bar within 600 ms. One, both or none of the distracter stimuli could change color before the target (250 ms after cue onset to 400 ms before the target or another distracter color change) at any given trial. If the monkey released the bar to the distracter change, failed to maintain fixation, or did not respond to the target color change within the specified time, the trial was aborted.

Receptive fields (RFs) were mapped by moving flashing stimuli throughout the visual field while the monkey was fixating centrally. In both FEF and V4, electrodes were advanced until clear visual responses could be elicited. A memory guided saccade

task was used to identify cells with visual responses and further characterize their RFs. Briefly, the trial started with the monkey fixating a central fixation spot. A stimulus flashed for 100 ms in one of six positions which were arranged on a circle with radius equal to the eccentricity that elicited the maximal response in the RF mapping task. After 750 ms and while the monkey was still fixating centrally, the fixation spot was extinguished and the monkey was rewarded for making a saccade to the memorized position of the peripheral stimulus.

For tests of attentional effects with non-overlapping RFs, we typically studied FEF sites with RFs confined in the upper quadrant and V4 sites with RFs confined in the lower quadrant of the same hemifield.

Recording

Spikes and local field potentials (LFPs) were recorded from FEF and V4 simultaneously using a Multichannel Acquisition Processor system by Plexon Inc. On a given day up to four tungsten microelectrodes were advanced through the dura in each area. Electrodes within an area were spaced 650 or 900 μm apart. Each electrode's signal was passed through a headstage with gain one and a high input impedance (Plexon Inc, HST/8o50-G1) before extracting the spike and LFP components. In a subset of recordings, a headstage with gain 20 and a lower input impedance was used (Plexon Inc HST/8o50-G20). Signals were filtered between 250 Hz-8 kHz, amplified and digitized at 40 kHz to obtain spike data. Spikes were selected offline to include multi-unit activity on each electrode by setting a threshold that separated spikes from noise. For the LFP, the signals were filtered between 0.7-170 Hz, amplified and digitized at 1 kHz. LFP data were post-processed to correct for the known phase shifts which are induced by the filters in the system and affect mainly low frequencies (see below) (*S1*).

The location of recordings in both FEF and V4 was verified at the end of the experiments with MRI. Electrodes placed into representative recording sites were visible in the MRI because the artifact induced by the titanium head post and screws did not obscure the cortex under the plastic recording chamber. The FEF recordings were in the anterior bank of the arcuate sulcus, and the V4 recordings were on the prelunate gyrus. In one monkey, we electrically stimulated in FEF and elicited eye movements.

Data Analysis

To correct for phase shifts in the LFP signals, we followed a procedure similar to that described in *(S1*). Briefly, using a waveform generator sinusoidal signals of known frequencies (from 0.5 HZ to ~400Hz) were injected into two channels one through the headstage and preamplifier used in recordings (subjected to the same filtering that the field potential signal was subjected to at the time of recording) and one going directly to an A/D channel with no filtering. The mean phase difference between the two signals was calculated for each frequency using the Hilbert transform and the filters' response function was determined. The empirically derived digital filter was applied to the recorded data in time reverse order to cancel the potential time delays caused by the original filters. We also used the utility program provided by Plexon Inc to correct for

the filter induced time delays (FPAlign, http://www.plexoninc.com/support/softwaredownloads.html). Results from the two methods were similar. In the subset of recordings performed with the HST/8o50-G20 headstage, which can introduce additional time delays due to a voltage divider effect depending on the impedance of the recording electrodes, we followed the same procedure using electrodes that had been used for recordings (and thus their impedance was similar to that during the recording). We found that the induced time delays did not differ very much for different electrodes of the same type. Moreover, our phase results were not different for the two subsets of recording data where the two different headstages were used.

Firing Rate Analysis. Firing rates were computed for sites that showed a significant visual response (Wilcoxon rank-sum test, $p < 0.05$). The interval used for the statistical comparison was 50-250 ms after stimulus onset for the post-stimulus period and -200-0 ms relative to stimulus onset for the pre-stimulus period. Only data from days when simultaneous recordings in FEF and V4 were carried out were included in the analysis (292 sites with visual responses in the FEF – 88 in monkey 1 and 204 in monkey 2 - and 262 sites in V4 – 82 in monkey 1 and 180 in monkey 2). The RF location of a multi-unit spike signal in each area was defined to be the location that elicited the maximal visual response in the memory guided saccade task. Signals were rejected if they showed significant response at the stimulus location in the opposite hemifield.

Attentional effects were assessed by comparing neuronal responses in trials where attention was directed inside the RF to responses in trials where attention was directed outside the RF to the stimulus in the opposite hemifield. For all statistical comparisons throughout the paper significance values below the 0.001 level are reported at this cutoff point. Firing rate data were normalized to the mean pre-cue activity (-200-0 ms relative to cue onset) across both conditions (attention inside the RF and attention outside the RF). To assess the latency of attentional effects, responses were averaged in 10 ms non-overlapping windows, and significant differences between the two conditions were determined in each bin for each site across trials using a Wilcoxon rank-sum test ($p < 0.05$). The latencies based on the population-level data were determined by averaging across sites instead of trials, using the mean trial-averaged value in each bin for each electrode and assessing statistical significance with a Wilcoxon sign-rank test ($p < 0.05$). The latency of the attentional effect was defined to be the first of three consecutive bins that were all significantly different in the two attentional conditions. The distributions of latencies for individual sites were compared using a Wilcoxon rank-sum test.

To test whether the difference in the latency estimates at the population level in the two areas was statistically significant we conducted a permutation test with resampling. The null hypothesis was that the latency at the population level was not different in the two areas. We randomly selected a number of signals equal to our FEF population from a pool of signals consisting of all (FEF and V4) recorded signals. The selected signals from the pool were arbitrarily labeled as FEF signals whereas the remaining signals (equal in size to our V4 population) were arbitrarily labeled as V4 signals. The population latency was determined for each group ($lat_{pseudoFEF}$ and $lat_{pseudoV4}$) by averaging the firing rate data across the sites assigned in each group and employing the three consecutive

significant 10 ms bins approach described above. We calculated the difference between the two latencies $\Delta lat_{pseudo(FEF-V4)} = lat_{pseudoFEF} - lat_{pseudoV4}$. We used $\Delta lat_{pseudo(FEF-V4)}$ as the statistic to test the null hypothesis. We repeated the resampling process 10,000 times. The generated distribution of 10,000 values of the statistic ($\Delta lat_{pseudo(FEF-V4)}$) estimates the sampling distribution under the condition that the null hypothesis is correct. We subsequently located the value of the difference we actually observed ($\Delta lat_{real(FEF-V4)}$) on the permutation distribution in order to determine the probability that we would observe a value at least as large as the observed value if the null hypothesis were correct. That is, we asked what percentage of data points in the permutation distribution was equal to or greater than the observed value. To employ a two-sided test, we considered the absolute latency difference.

Coherence Analysis. We calculated spike-LFP, spike-spike and LFP-LFP coherency, which is a measure of phase locking between two signals as a function of frequency. To achieve optimal spectral concentration we used multi-taper methods for spectral estimation providing a smoothing of ±10Hz in frequencies above 25Hz and ±3Hz for lower frequencies. An optimal family of orthogonal tapers given by the discrete prolate spheroid sequences (Slepian functions) was used as described before *(S2-S4*). Coherency for two signals x and y is calculated as

$$Cxy(f) = \frac{Sxy(f)}{\sqrt{(Sx(f)Sy(f))}}$$

where Sx(*f*), and Sy(*f*) represent the auto-spectra and Sxy(*f*) the cross-spectrum of the two signals x and y. Auto-spectra and cross-spectra are averaged across trials before the coherency calculation. Coherency is a complex quantity with its absolute value, called coherence, ranging from 0 (when there is no consistent phase relationship between the two signals) to 1 (when the two signals have a constant phase relationship).

The same number of trials for each condition (attention inside the RF, attention outside the RF) was used for the calculation of coherence for a given pair of recording sites. Moreover, the length of data included in each condition was the same in each pair of sites. These steps eliminated any possible bias from differing sample sizes. Data from 300 ms after cue onset up to the earliest color change (target or distracter) in each trial were included in the coherence analysis, provided that this window was at least 400 ms.

All coherence calculations used the data from two different electrodes, to preclude the possibility that spikes would actually contribute to the LFP recorded on the same electrode. For the calculation of coherence within each area, only data from days when simultaneous recordings in FEF and V4 were carried out were used. Spikes from any given site were included in the analysis only if the multi-unit activity showed visual responses to the onset of the stimuli in the attentional task (similar to the selection of spike signals for the firing rate analysis) and showed statistically significant sustained visual activity relative to the baseline (Wilcoxon rank-sum test, $p < 0.05$) in a window that started 200 ms before the target color change and ended at the target color change. To distinguish between sites with overlapping and non-overlapping RFs, RF locations

were assessed separately for spike signals and LFP signals. RF location for multi-unit spike signals was determined as described above for the firing rate analysis. The RF location of the LFP was determined from the memory guided saccade and was defined as the location with the maximal absolute peak value of the LFP within 400 ms after the onset of the stimulus.

The measure of coherence we used is designed to be invariant over changes in firing rates. However, coherence and other correlational measures can be affected by issues such as the signal to noise ratio of recorded signals, particularly at low ratios, and this could in principle be influenced by firing rate. To eliminate any possible contribution of firing rate differences to these values, we equated firing rates across conditions for the coherence analyses using the following procedure. Spike trains in both attend-in and attend-out conditions were convolved with a Gaussian kernel (sigma=10 ms), and firing rate was averaged across trials for each condition. We calculated the difference in rates at each time bin and divided by the maximum rate in the two conditions at that bin. This allowed us to determine the probability in each bin that spikes would need to be removed from the higher firing rate signal. Spikes in the original spike trains were randomly removed based on the fixed probability value. For example, a difference of 50% between the two conditions in a given millisecond would result in a 50% probability that an existing spike would be removed from the condition with the higher firing rate on that millisecond on a given trial. Equating spikes this way between the two attention conditions typically resulted in a reduction in absolute coherence values of the attended condition by 6-10% and a similar consequent reduction in coherence differences across conditions.

To check if any of the coherence measured between two sites resulted from stimulus-locked oscillations, we shuffled the order of trials for one of the signals, e.g. the LFP, within each condition for each pair. This analysis eliminated the observed coherence effects (see Shuffled Trials results section below).

Spike Triggered Average (STA) of the LFP: STAs were calculated by averaging LFP segments ±100 ms around every recorded spike in each condition. The same spike-field pairs that were used in the coherence analysis were included in the STA of the LFP analysis. The first 300 ms after cue onset were not included in the analysis in order to exclude any transient deflections in the LFP. Accordingly, we included in the analysis only spikes that occurred from 400 ms after cue onset to 100 ms before the time of the first color change. The average across all recorded pairs of spike-LFP channels showed clear gamma oscillations together with lower frequency modulation. To display more clearly the average relative phase of spikes, the STA was filtered using a bandpass filter (35-80 Hz) with zero phase distortion. Visual inspection of the original broad-band and filtered signals verified that no distortion was introduced. The Hilbert transform was used to determine the relative phase of the filtered STAs of the LFP at time zero i.e. at the time the spikes occurred (Fig. S3)

LFP power: Coherence measures are a poor choice to evaluate precise onsets in time because their calculation requires a reasonable time window for analyses. We therefore, used the Hilbert-Huang Transform (HHT) for LFP power estimation across time *(S5*).

The advantages of this method over traditional spectrogram methods employing sliding windows have been discussed previously *(S5, S6*). Briefly, the method allows for the analysis of non-stationary time series and provides a better temporal and frequency resolution compared to Fourier analysis. This is achieved by employing the Empirical Mode Decomposition (EMD) method, together with the Hilbert transform. The EMD method decomposes the signal (in this case the LFP) into a small number of narrow band components (intrinsic mode functions, IMF) by identifying the time scales that are intrinsic to the time series. A signal is considered to be an IMF if the number of its local extrema and the number of its zero crossings is either the same or differ by one. Because of their properties (locally symmetrical, absence of riding waves) the IMFs can be subjected to the Hilbert transform to obtain meaningful instantaneous frequency information. The resulting Hilbert spectrum represents amplitude and instantaneous frequency as a function of time.

The Hilbert spectrum was calculated as described above for each trial employing matlab functions provided with the Hilbert-Huang Transform Data Processing System software toolkit (HHT-DPS v1.4.10) developed by the National Aeronautics and Space Administration, at Goddard Space Flight Center (http://techtransfer.gsfc.nasa.gov/HHT/).

The resulting three dimensional time-frequency spectra were smoothed using a 2D Gaussian filter (sigma = [4ms, 2Hz], size = [10ms, 5Hz]). To obtain latency estimates of the attentional modulation in each signal we first determined the largest value of LFP power across the two attention conditions within a frequency range 30-140 Hz for each time bin. LFP gamma power was obtained after averaging within a 20 Hz window around the frequency with the maximum LFP power for the same bin. The attentional latency was determined as the time corresponding to the first out of three consecutive 10 ms bins that were significantly different in the two conditions (Wilcoxon rank-sum test, $p < 0.05$). To compute the population average, the LFP gamma power per condition for each signal was normalized to the average gamma power across both conditions in a 200 ms window before cue onset. The attentional latency at the population level was estimated using the same criteria as for individual signals with a Wilcoxon sign-rank test. Moreover, we tested whether the estimated latencies at the population level were statistically different in the two areas by employing a permutation test similar to the one described for the firing rate attentional latencies.

Directional Influences

Granger causality Analysis: To measure directional influences between the FEF and V4 we employed Granger causality spectral analysis using parametric methods of spectral estimation. According to Granger *(S7*), at a given point in time we can say that one stochastic process (X_t) is "causal" to a second stochastic process (Y_t) if the autoregressive predictability of Y_t is improved by the inclusion of past values of X_t. To evaluate the relative strengths of influences between the two areas in the two directions (FEF to V4 and V4 to FEF) we followed the approach described in *(S8, S9*). This approach is based on the use of multivariate autoregressive time series models for the estimation of spectral quantities.

Briefly, as described in *(S8)*, the bivariate autoregressive model (AR) for a pair of LFP recordings (FEF-V4) at time t (X_t) can be written as

$$\sum_{k=0}^{m} A_k X_{t-k} = E_t$$

where m is the order of the model, A_k the 2x2 coefficient matrices and E_t the residual error with covariance matrix Σ. As a preprocessing step in our analysis, we subtracted the ensemble mean from each trial in every recording site and divided by the standard deviation *(S9, S10)*. This way (a) the first-order nonstationarity is removed from the data and (b) the ensemble of single-trial time series can be considered a stochastic process with zero-mean, as it is required for the autoregressive modeling method *(S10)*. To determine the relative strength of directional influences, granger causality values were computed for each condition using a single 500 ms window starting at the time of cue onset. Moreover, to test the temporal evolution of the directional influences we conducted a separate analysis in successive windows of 150 ms advanced every 10 ms with the first window starting 275 ms before the cue onset. By using short, highly overlapping time windows we can consider that the underlying stochastic processes are locally stationary. We used a total of 121 windows. For each window segment and for each pair of LFP signals the parameters of the AR model were estimated using the Burg algorithm for vectors (Nuttall-Strand method) and the model's optimal order was determined using the Combined Information Criterion *(S11, S12)*. The model's parameters (partial correlations matrices and the covariance matrix) were estimated for each trial separately and they were subsequently averaged across trials. Test for stationarity included determining whether the set of partial correlations defined a stationary process. With the model coefficients A_k and Σ estimated, the spectral matrix can be calculated:

$$S(f) = H(f)\Sigma H^*(f)$$

where * represents matrix transposition and complex conjugation and H(*f*) is the transfer function $(H(f) = \left(\sum_{k=0}^{m} A_k e^{-2\pi i k f}\right)^{-1})$. The individual power spectra and cross spectra are elements of the 2x2 spectral matrix S(*f*) e.g. the power spectrum of channel 1 would be given by element $S_{11}(f)$, that of channel 2 by $S_{22}(f)$ etc.

According to *(S13)*, the power at a given frequency for a given site consists of an intrinsic part and a part that can be predicted by the power from another site. Accordingly, one can define the Granger causality at each frequency as the ratio of predicted power to total power. In mathematical terms the Granger causality spectrum is defined for each direction of influence for the two LFP time series (1 and 2 or FEF and V4 in this case) as *(S8, S13)*:

$$I_{2\to 1} = -\ln\left(1 - \frac{\left(\Sigma_{22} - \frac{\Sigma_{12}^2}{\Sigma_{11}}\right)|H_{12}|^2}{S_{11}(f)}\right)$$

$$I_{1\to 2} = -\ln\left(1 - \frac{\left(\Sigma_{11} - \frac{\Sigma_{12}^2}{\Sigma_{22}}\right)|H_{21}|^2}{S_{22}(f)}\right)$$

with Σ_{11}, Σ_{22}, Σ_{12} elements of Σ.

Granger causality spectral values were obtained as described above for each direction and each attentional condition in subsequent windows over time. The designation of time corresponds to the center of each window. Data for each direction were normalized to the mean value between 40 and 60 Hz across both conditions -200 to 0 ms relative to cue onset. To estimate attentional latency Granger causality values in the gamma range (40-60 Hz) were averaged. The latency of the attentional effect for a given direction was estimated as the point in time where the first out of ten consecutive data points (spaced 10 ms apart) was significantly different between the two attentional conditions (paired t-test $p < 0.05$). A permutation test was employed to test whether the obtained latency estimates for the two directions were significantly different as described in the firing rate analysis.

Moreover, to evaluate statistical significance in the Granger spectra we identified gamma Granger peaks in the time-averaged spectra calculated in the fixed 500 ms window and we assessed significance using a permutation procedure. Briefly, for each pair of signals we shuffled the trial order for the second LFP signal. This way we generated a distribution of Granger spectral values expected by chance. The peak gamma Granger values obtained from the original data were compared to this distribution.

Supporting text

Behavioral performance

The monkeys performed with 84% hits on the target change (monkey 1: 87%, monkey 2: 82%) and 2% false alarms to the distracter change (monkey 1: 4%, monkey 2: 1%).

Attention effects on firing rate

More than 85% of the FEF recorded signals showed an enhancement with attention (chi-square $p < 0.001$) with a median increase of 16% for all neurons. Similarly, more than 94% of V4 recorded signals displayed enhanced responses with attention (chi-square $p < 0.001$) with a median increase of 13% for all neurons (Fig. S1).

Latency of attentional effects on firing rate data

To rule out the possibility that earlier latencies in the FEF firing rates might be due to the larger attentional effect in FEF compared to V4 in the first 300 ms after cue onset, we carried out a control analysis including only multi-unit signals with attentional effects of similar size. Signals that showed 20-40% increase with attention 100-350 ms after cue onset (35 signals in V4 and 85 signals in FEF) were included. As with the entire population, this subset of signals showed that the distribution of latencies in FEF signals was shifted earlier compared to that in V4 (FEF median: 181 ms, V4 median: 281 ms; Wilcoxon rank-sum test, $p < 0.001$).

Attention effects on coherence

More than 66% of the recorded spike-LFP pairs in V4 and more than 64% of the pairs in FEF showed an increase in spike-field coherence in the gamma range, with a median increase of 14% and 16% in V4 and FEF, respectively. Across the two areas, more than 60% of the recorded pairs showed enhancement in coherence with attention (chi-square, $p < 0.001$ for both pair types; V4 spikes – FEF LFPs, median increase 16%; FEF spikes – V4 LFPs, median increase 22%). Similarly, more than 85% of the LFPs pairs recorded across the two areas showed an enhancement with attention with a median increase of 61% for all pairs (Fig. S2).

Spatial selectivity in coherence

Coherence was also computed between spikes in FEF and LFPs in V4 for sites with non-overlapping RFs. We considered only FEF spike- V4 LFP pairs with FEF sites having RFs confined in the upper quadrant as indicated by the lack of a significant visual response to stimuli in the lower quadrant in the memory guided saccade task (prestimulus -150-0 ms, poststimulus 50-200 ms relative to stimulus onset; rank-sum test $p > 0.05$) and V4 sites with RFs confined in the lower quadrant. We found 47 such pairs, 27 of which also showed significant sustained activity in the attentional task. The result is shown in

Figure 2F of the main text and shows no significant differences (40-60 Hz, one way ANOVA, $p = 0.86$) among the two attention conditions (attention directed to the V4 RF, attention directed to the stimulus on the right hemifield) and the pre-stimulus period. Similar results were obtained for the condition where attention was directed in the upper quadrant.

Effect of attention on phase relationships

The relative phase of gamma coherence between spikes and LFPs was obtained for both attention conditions. Attention had no effect on these time/phase shifts, with a similar distribution of shifts observed in both attend-in and attend-out conditions (Kolmogorov-Smirnov test, FEF, $p = 0.17$; V4, $p = 0.82$; FEF spikes – V4 LFPs, $p = 0.70$; V4 spikes – FEF LFPs $p = 0.62$). The values for the attend-in condition are reported in the main text whereas here we report those for the attend-out condition for comparison: FEF, median phase = 0^o; V4, median phase = -19^o; FEF spikes - V4 LFPs, median phase = -152^o; V4 spikes - FEF LFPs, median phase = 140^o).

Shuffled trials

To rule out the possibility that any correlations reflected in coherence between the two areas arise from stimulus-locked responses, we conducted a control analysis which involved shuffling of trials for the LFP signals while maintaining the order of the trials for the spike channels. The analysis was performed in a window 400 ms to 1200 ms after cue onset. Coherence peaks were eliminated (Fig. S4) and the distribution of relative phases in the gamma range between spikes and shuffled LFPs across the two areas showed no preferred phase (Kuiper's test FEF spikes – V4 LFPs, attend in: $p = 0.10$, attend out $p = 0.09$; V4 spikes – FEF LFPs, attend in: $p = 0.12$, attend out $p = 0.07$). This finding confirms that the correlation and timing relationship between the two areas is not merely a result of stimulus-locked responses in the two areas.

Supporting References

S1. M. J. Nelson, P. Pouget, E. A. Nilsen, C. D. Patten, J. D. Schall, *J Neurosci Methods* 169, 141 (2008).
S2. P. Fries, T. Womelsdorf, R. Oostenveld, R. Desimone, *J Neurosci* 28, 4823 (2008).
S3. M. R. Jarvis, P. P. Mitra, *Neural Comput* 13, 717 (2001).
S4. B. Pesaran, M. J. Nelson, R. A. Andersen, *Nature* 453, 406 (2008).
S5. N. E. Huang *et al.*, *Proceedings of the Royal Society of London Series a-Mathematical Physical and Engineering Sciences* 454, 903 (1998).
S6. H. Liang, S. L. Bressler, E. A. Buffalo, R. Desimone, P. Fries, *Biol Cybern* 92, 380 (2005).
S7. C. W. J. Granger, *Econometrica* 37, 424 (1969).
S8. A. Brovelli *et al.*, *Proc Natl Acad Sci U S A* 101, 9849 (2004).
S9. Y. Zhang, Y. Chen, S. L. Bressler, M. Ding, *Neuroscience* 156, 238 (2008).
S10. M. Ding, S. L. Bressler, W. Yang, H. Liang, *Biol Cybern* 83, 35 (2000).
S11. S. de Waele, P. M. T. Broersen, *Ieee Transactions on Signal Processing* 51, 427 (2003).
S12. S. L. Marple, *Digital Spectral Analysis with Applications*. (Prentice-Hall, Englewood Cliffs, NJ, 1987).
S13. J. Geweke, *Journal of the American Statistical Association* 77, 304 (1982).

Figure S1

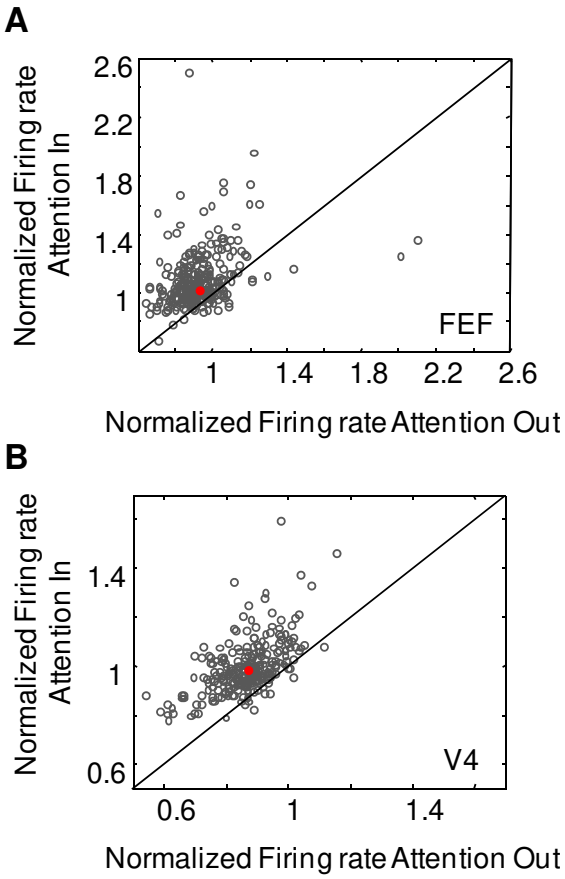

Fig. S1 Distribution of mean normalized firing rate 100-800 ms following cue onset with attention inside (y-axis) and attention outside (x-axis) the RF of the recorded neurons. **(A)** Effect of attention in FEF neurons **(B)** Effect of attention in V4 neurons. Each point represents one signal. The red circles indicate the median of the distributions. Points above the diagonal indicate a positive attentional effect (higher response with attention) whereas points below the diagonal indicate a negative attentional effect (lower responses with attention).

Figure S2

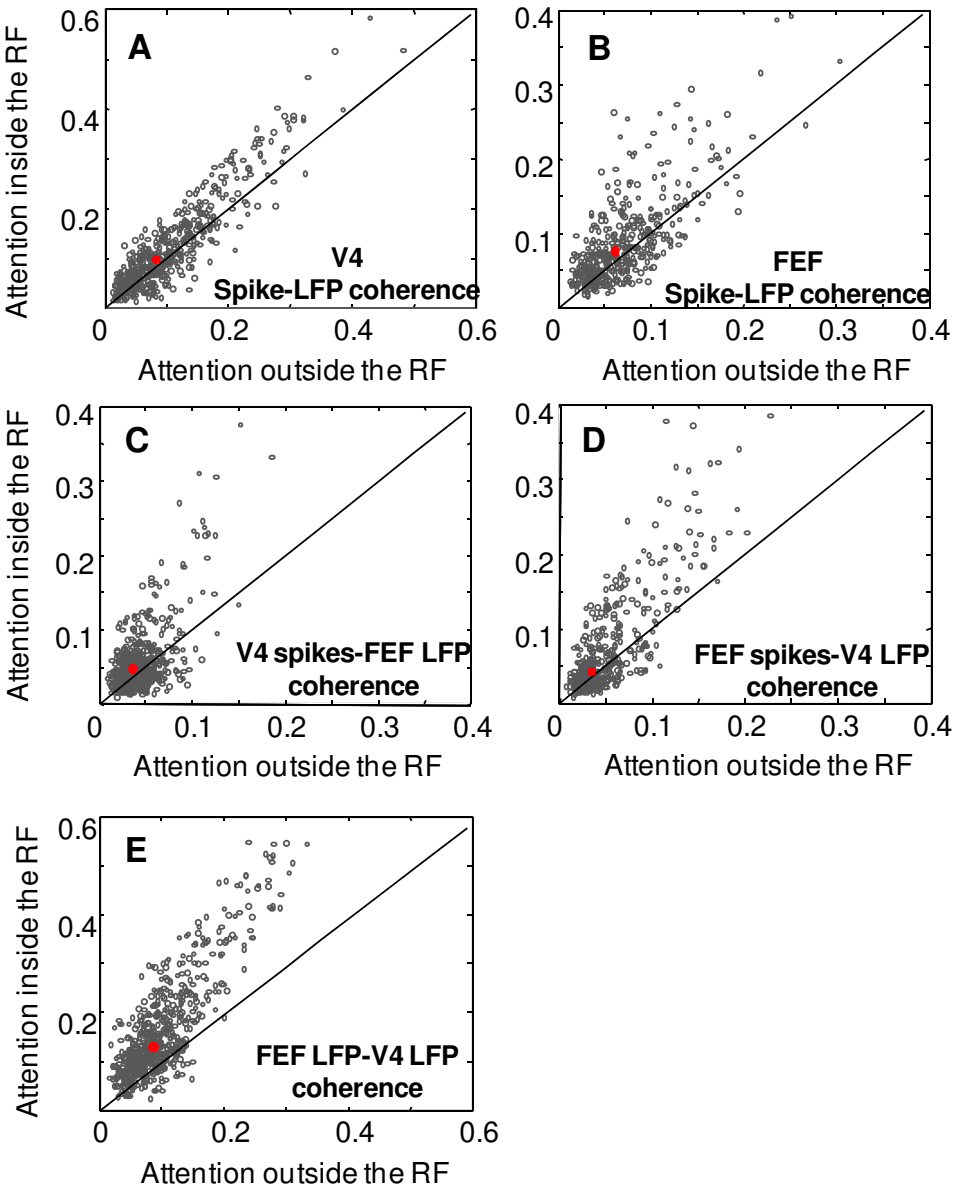

Fig. S2 Distribution of average coherence (40-60 Hz) with attention inside (y-axis) and attention outside (x-axis) the RF of the recorded signals **(A)** V4 spike-LFP coherence, **(B)** FEF spike-LFP coherence, **(C)** V4 spike-FEF LFP coherence, **(D)** FEF spike-V4 LFP coherence and **(E)** FEF LFP-V4 LFP coherence. Each point represents one spike-LFP (or LFP-LFP) pair. The red circles indicate the median of the distributions. Points above the diagonal indicate a positive attentional effect (higher coherence with attention) whereas points below the diagonal indicate a negative attentional effect (lower coherence with attention).

Figure S3

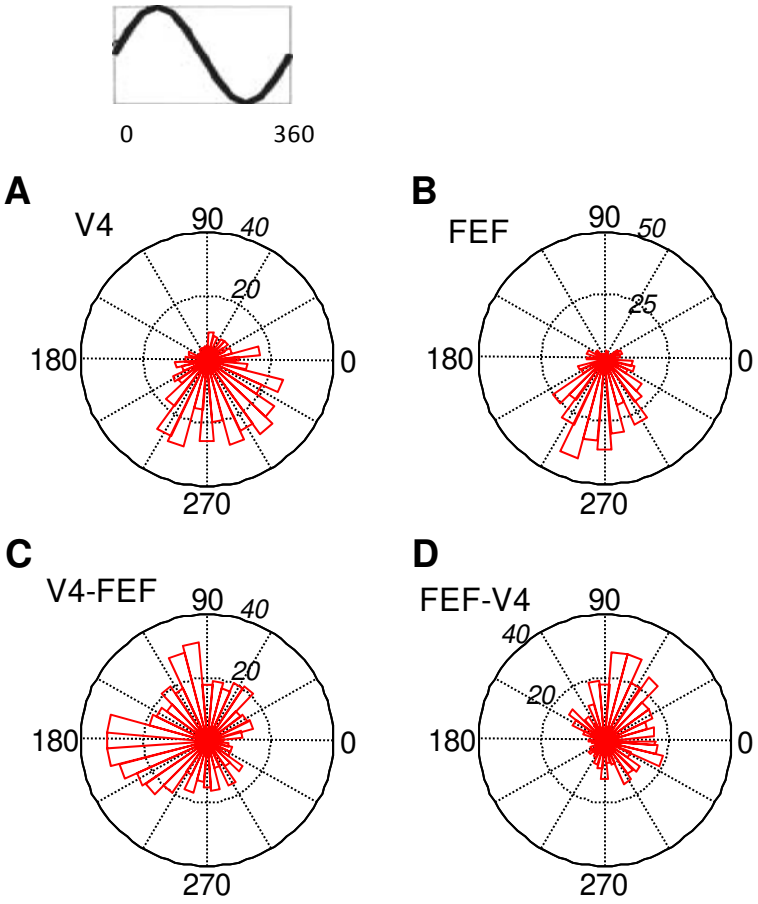

Fig. S3 Distribution of relative phase of the STA of the LFP at spike occurrence. **(A)** Distribution of phases of STA of the V4 LFPs to V4 spikes, **(B)** Distribution of phases of STA of the FEF LFPs to FEF spikes, **(C)** Distribution of phases of STA of the FEF LFPs to V4 spikes, and **(D)** Distribution of phases of STA of the V4 LFPs to FEF spikes. The inset on top illustrates a sine wave to indicate that phase values were calculated assuming a sine function for the gamma oscillation of the STA of the LFP. According to this convention the maximum negativity in the gamma oscillation corresponds to a phase value of $3\pi/2$ rad or 270^{o}. Note an approximately half a cycle phase shift when comparing within to across areas phase relationships.

Figure S4

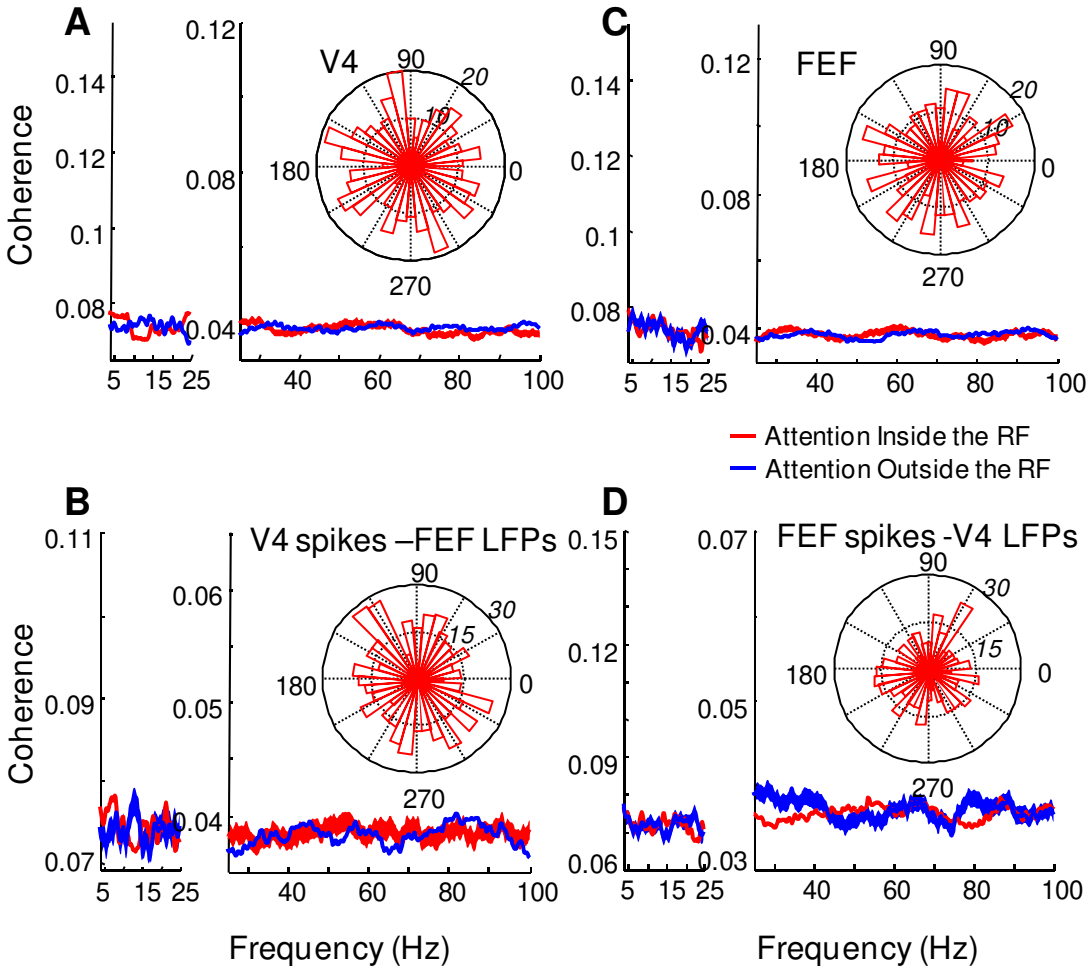

Fig. S4 Spike-field coherence and phase relationships after shuffling the LFP data. Spike field coherence **(A)** within V4, **(B)** within FEF, **(C)** between spikes in V4 and LFPs in FEF, and **(D)** between spikes in FEF and LFPs in V4. Conventions as in Fig. 2. Tapers providing an effective smoothing of ±10 Hz were used for spectral estimation of higher frequencies (25-100 Hz, right part of each graph) and tapers providing smoothing of ±3Hz were used for lower frequencies (<25 Hz, left part of each graph). Insets show the distribution of average relative phases (40-60 Hz) for the condition where attention was directed inside the RF of the recorded sites.

Figure S5

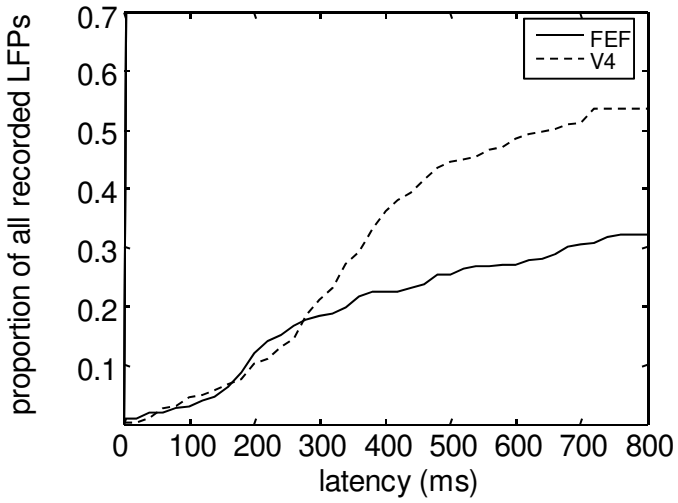

Fig. S5 Cumulative distribution of LFP gamma power attentional latencies in FEF (solid line) and V4 (dashed line). Distributions are shown as proportion of sites out of all recordings in each area.

	FEF	**V4**
Firing rate (population average), earliest latency	80 ms	130 ms
Firing rate, median of latency distribution	160 ms	250 ms
LFP gamma power (population average), earliest latency	120 ms	100 ms
LFP gamma power, median of latency distribution	200 ms	210 ms
	FEF→V4	**V4→FEF**
Granger causality (population average), earliest latency	110 ms	160 ms

Table S1. Latencies of attentional effects on firing rates, LFP gamma power, and Granger causality values. Latency values obtained from the average of all population data reflect the earliest latency measured in the population. Median latencies are from the distributions of all individual latencies, measured within the first 300 ms postcue onset.